

An enhanced finite element method for two dimensional linear viscoelasticity using complex Fourier elements

Seyed Ali Ghazi Mirsaed* and Vahidreza Kalatjari

Faculty of Civil Engineering, Shahrood University of Technology, Shahrood, Iran

ARTICLE INFO

Article history:

Received: 30 August 2018

Accepted: 21 October 2018

Keywords:

Viscoelasticity

Finite element method

Complex Fourier shape functions

Shape parameters

Complex Fourier elements (CFEs)

ABSTRACT

In this paper, the finite element analysis of two-dimensional linear viscoelastic problems is performed using quadrilateral complex Fourier elements and the results are compared with those obtained by quadrilateral classic Lagrange elements. Complex Fourier shape functions contain a shape parameter which is a constant unknown parameter adopted to enhance approximation's accuracy. Since the iso-parametric formulation utilized in the finite element code, based on the experience of authors, it is proposed that a suitable shape parameter for each problem is adopted based on an acceptable approximation of the problem's geometry by a complex Fourier element. Several numerical examples solved, and the results showed that the finite element solutions using complex Fourier elements have excellent agreement with analytical solutions, even though noticeable fewer elements than classic Lagrange elements are employed. Furthermore, the run-times of the executions of the developed finite element code to obtain accurate results, in a same personal computer, using classic Lagrange and complex Fourier elements compared. Run-times indicate that in the finite element analysis of viscoelastic problems, complex Fourier elements reduce computational cost efficiently in comparison to their classic counterpart.

1. Introduction

The viscoelastic behavior of structures, such as the vibration of aerospace craft, the stress analysis of solid propellant rocket motor, the creep analysis of concrete buildings and the design of a turbine blade is of vital importance in engineering design. In particular, the damping effect of the viscoelastic material can be utilized to diminish the vibration of structures [1]. Employment of the theory of elasticity to simplify the analysis proves to be inconsistent with the accurate behavior of materials since most engineering materials display much time dependency due to internal friction [2]. Hence, viscoelastic constitutive relations should be adopted rather than elastic constitutive relations regarding the behavior of materials. There are many works in the literature on the theory of Viscoelasticity such as Flugge [3], Christensen [4], Brinson [5], Gutierrez-Lemini [6], Tschoegl [7]. In structural analysis of time-dependent materials, conventionally linear viscoelasticity has been employed. There are fundamentally three approaches that may be adopted in a linear viscoelastic analysis: Laplace transformation, Fourier transformation, and direct time integration method [2, 8, 9]. Analytical solutions to the equations of viscoelasticity are

generally obtained by the implementation of the correspondence principle. These methods take advantage of the fact that the governing equations of viscoelasticity can be converted to the governing equations of elasticity by using integral transformations [1]. Hence, if an explicit solution to the associated equations of elasticity is available, then the solution of that viscoelasticity can be found by inversion of the Laplace transform. The demerit of this approach is that it can only solve a narrow class of problems for which it is possible to obtain an explicit solution to the associated equations of elasticity [10]. Flugge [3] applied the Laplace transform to viscoelastic beams. Christensen [4] presented the application of the Fourier transform to viscoelastic beams. Sorvari and Hamalainen [11] analyzed and compared the time integration method in linear viscoelasticity [2].

Since there are often no closed-form solutions for the problems with complex geometries, loading conditions and constitutive relations, numerical solution approaches should be adopted. Finite element method (FEM) and boundary element method (BEM) are the most prevalent techniques in solving viscoelastic problems among several numerical methods [2].

* Corresponding author. Tel.: +98-21-46130889; [e-mail: alighazi@shahroodut.ac.ir](mailto:alighazi@shahroodut.ac.ir)

Implementation of the FEM to the solution of static and dynamic problems incorporating materials exhibiting viscoelastic behavior has been evolved over recent decades [2]. The FEM has been applied to viscoelasticity problems by several researchers. To the best of authors' knowledge, King [12] developed the first viscoelastic FE code. The application of this program was restricted to plane stress and plane strain conditions. The theory was developed utilizing Boltzmann hereditary integral representations of constitutive equations in terms of creep compliance. The essential assumptions in this approach were that the creep compliance could be split into an elastic part and a creep part, and the strain could be assumed to remain constant within a time step [13].

Ghazlan et al. [10] developed an incremental formulation in time domain for the displacement and stress analysis of quasi-static, linear, thin viscoelastic structures undergoing mechanical deformation. By using a discrete creep spectrum, they represented the viscoelastic behavior of a material by incremental constitutive equations. Zocher et al. [13] developed a numerical algorithm for the solution of the uncoupled, quasi-static initial/boundary value problem involving orthotropic linear viscoelastic media undergoing thermal and mechanical deformation. They used an integral form of constitutive equation involving the relaxation moduli, which is transformed into an incremental algebraic form, prior to the development of the FE formulation. The relaxation moduli has been represented by a Dirichlet-Prony series that leads to derive a recursive relationship after incrementalization.

It is crucially important to choose the type of shape functions as interpolation tools in FEM. Classic Lagrange shape functions usually have been employed in conventional FEM. It just has been relied upon the increasing the degree of these shape functions in complicated problems, if necessary. In this study, the application of a specific type of modern shape functions, called complex Fourier, in FE analysis is investigated.

Complex Fourier shape functions, which derive from complex Fourier radial basis functions (RBF), were implemented in solving two-dimensional potential problems using BEM by Khaji and Hamzehei Javaran [14]. Recently, Hamzehei-Javaran employed complex Fourier shape functions to approximate the state variables of Navier's differential equation in transient dynamic problems by using FEM [15]. In the present study, the application of FEM, in solving viscoelastic problems, is developed by adopting complex Fourier elements, hereinafter referred to as CFEs in the article, in the 2D domain. Both complex Fourier RBFs and shape functions contain shape parameters because the latter is derived from the enrichment of the former. In order to adapt CFEs with the optimum shape functions, we should find a way for the estimation of shape parameters in complex Fourier shape functions.

For the demonstration of the validity and accuracy of the proposed elements, some numerical examples with available analytical solutions are presented. Convergence of FE solutions in some examples is also examined. It is verified that the patch test is passed by CFEs to guarantee the convergence of solutions.

The influence of the number of CFEs on the convergence toward a common solution (analytical or numerical) is compared with classic Lagrange elements to assess accuracy and robustness of these elements in FE analysis of viscoelastic problems. It is forecast that CFE is much more robust than classic Lagrange element because the former satisfies trigonometric, exponential and polynomial function fields simultaneously, while the latter only satisfies polynomial function fields. This paper is organized as follows: FE formulations for viscoelasticity, which are adopted

in this study, are explained in Section 2. Complex Fourier RBFs are briefly introduced in Section 3. Radial point interpolation method, which is generally used in meshless methods, is described in Section 4. In Section 5, CFEs are derived, and their properties are discussed in Section 6. In Section 7, an essential discussion about shape parameters in CFEs are presented, and an approach for the approximation of the shape parameters based on the experience of the authors is proposed. Some illustrative examples are studied in Section 8. Finally, Section 9 draws the conclusion.

2. Finite element formulation adopted for linear viscoelasticity

Based on Boltzmann hereditary integral [3-7], mathematical expression of viscoelastic constitutive equation is given by [13, 16]:

$$\sigma_{ij}(\tau) = \int_0^\tau C_{ijkl}(\tau - \tau') \frac{\partial \varepsilon_{kl}(\tau')}{\partial \tau'} d\tau' \quad (1)$$

Where $\sigma_{ij}(\tau)$ and $\varepsilon_{kl}(\tau)$ are stress and strain tensors at time τ

, respectively. The term C_{ijkl} represents the fourth-order tensor of isotropic relaxation moduli, relating stress to strain. By converting the constitutive equation (1) into an incremental form, the following equation is obtained [13, 16]:

$$\Delta \sigma_{ij} = C'_{ijkl} \Delta \varepsilon_{kl} + \Delta \sigma_{ij}^R \quad (2)$$

Where C'_{ijkl} and $\Delta \varepsilon_{kl}$ are given below [13, 16]:

$$C'_{ijkl} = C_{ijkl_\infty} + \frac{1}{\Delta \tau} \sum_{q=1}^M \eta_{ijkl_q} (1 - e^{-\frac{\Delta \tau}{\rho_{ijkl_q}}}) \quad (\text{no sum on } i, j, k, l) \quad (3)$$

$$\Delta \varepsilon_{kl} = R_c \Delta \tau \quad (4)$$

$$\rho_{ijkl_q} = \frac{\eta_{ijkl_q}}{C_{ijkl_q}} \quad (5)$$

Where C_{ijkl_q} , η_{ijkl_q} and ρ_{ijkl_q} are spring constant, dashpot coefficient, and relaxation time of q -th Maxwell element, respectively and C_{ijkl_∞} is spring constant of the single spring element in Wiechert model as depicted graphically in Figure 1 [5]. Note that Einstein summation convention is not adopted in repeated indices. In equation (3), M is the total number of Maxwell elements in Wiechert model.

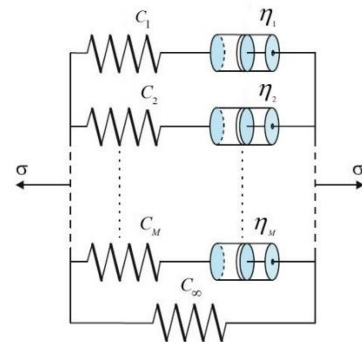


Figure 1. Wiechert model [5]

The timeline is subdivided into discrete intervals and the state of stress at time τ_n is known. In equation (4), R_ε is a constant, representing the time rate of change of strain over the time interval. This approximation is shown in Figure 2 [13].

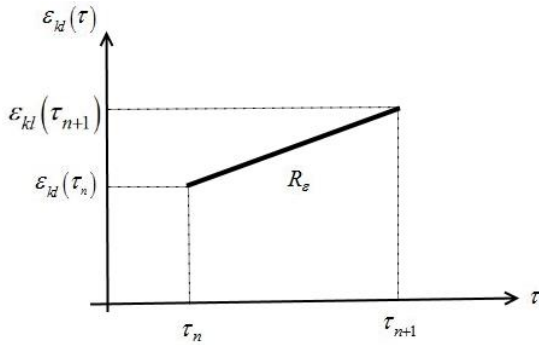


Figure 2. Approximation of $\varepsilon_u(\tau)$ over $\Delta\tau$ [13]

And $\Delta\sigma_{ij}^R$ is given by [13, 16]:

$$\Delta\sigma_{ij}^R = -\sum_{k=1}^3 \sum_{l=1}^3 Q_{ijkl} \quad (\text{no sum on } i, j) \quad (6)$$

Where [13, 16]:

$$Q_{ijkl} = \sum_{q=1}^M (1 - e^{-\Delta\tau/\rho_{ijkl}}) P_{ijkl}(\tau_n) \quad ; \quad (\text{no sum on } i, j, k, l) \quad (7)$$

$$P_{ijkl}(\tau_n) = e^{-\Delta\tau/\rho_{ijkl}} P_{ijkl}(\tau_n - \Delta\tau) + \eta_{ijkl} R_\varepsilon (1 - e^{-\Delta\tau/\rho_{ijkl}}) \quad (8)$$

; (no sum on i, j, k, l)

This incremental form of the constitutive equation is well suited to use in an FE code [13]. By applying the weighted residual method to the equilibrium equation as governing differential equation, and taking full advantage of incrementalized constitutive equation (2), after some algebraic manipulations, the FE formulation for one element is obtained as below [13, 16]:

$$[K^e][\Delta u^e] = [f_1^e] + [f_2^e] + [f_3^e] + [f_4^e] \quad (9)$$

with the following definitions of matrices [13, 16]:

$$\begin{aligned} [K^e] &= \int_{\Omega_e} [B^e]^T [C'^e] [B^e] d\Omega \\ [f_1^e] &= \int_{\Omega_e} [\Phi^e]^T \rho [f^{n+1}] d\Omega \\ [f_2^e] &= \int_{\Gamma_2^e} [\Phi^e]^T [T^{n+1}] d\Gamma \\ [f_3^e] &= \int_{\Omega_e} [B^e]^T [\sigma^n] d\Omega \\ [f_4^e] &= \int_{\Omega_e} [B^e]^T [\Delta\sigma^R] d\Omega \end{aligned} \quad (10)$$

It is noted that the domain and boundary of elements are denoted by Ω_e and Γ_e , respectively.

In equations (9) and (10), $[K^e]$ is referred to as the element stiffness matrix, $[\Delta u^e]$ is the vector of change in nodal displacement during $\Delta\tau$. $[f_1^e]$, $[f_2^e]$, $[f_3^e]$ and $[f_4^e]$ are contributions to the element load vector with respect to body forces, surface tractions, stresses at the start of the time step, and change of stresses during the time step $\Delta\tau$, respectively. In equations (10), $[B^e] = [\partial][\Phi^e]$, is strain-displacement (gradient) matrix. Where $[\partial]$ and $[\Phi^e]$ are derivation operator matrix and element shape functions matrix, respectively. ρ is the mass density, and $[f^{n+1}]$ and $[T^{n+1}]$ are element body force and element surface traction vectors at time τ_{n+1} , respectively. Finally $[\sigma^n]$ and $[\Delta\sigma^R]$ are vector of stress at the start of the time step and vector of change of stress during the time step, respectively [13, 16].

The governing global matrix equation, which results from the appropriate assembly of elements' contribution, is obtained by [13, 16]:

$$\{F\} = [K]\{\Delta u\} \quad (11)$$

Where $[K]$ is the global stiffness matrix, $\{F\}$ is the global load vector and $\{\Delta u\}$ is the change in the displacement vector during the time step $\Delta\tau$ [13].

3. Complex Fourier RBFs

Based on the definition of the Fourier series, any piecewise continuous periodic function $B(r)$ can be represented by a series of complex exponential functions as follows [14, 15]:

$$B(r) = \sum_{n=-\infty}^{+\infty} C_n e^{i\left(\frac{n\pi}{L}\right)r} \quad (12)$$

Where C_n and L are the usual parameters of complex Fourier series.

By assuming only one term of equation (12) as [14, 15]:

$$B(r) = \alpha e^{i\omega r} \quad (13)$$

In the above equation, r represents the Euclidean norm among data points, α and ω are shape parameters of complex Fourier RBFs which are constants that can be chosen to increase the approximation's accuracy. In this way, complex Fourier RBFs were obtained [14, 15].

4. Point Interpolation based on RBFs

Consider an approximation function $u(\mathbf{x})$ in an influence domain that consists of a set of arbitrary distributed nodes $P_i(\mathbf{x}_i)$, ($i = 1, 2, \dots, n$). n is the number of nodes in the influence domain of \mathbf{x} [16]. At the node \mathbf{x}_i , the nodal value of the function

is assumed to be u_i . Radial Point Interpolation Method (RPIM) constructs the approximation function $u(\mathbf{x})$ to pass through all these node points using radial basis function $B_i(\mathbf{x})$ and polynomial basis function $P_j(\mathbf{x})$ [17].

$$u(\mathbf{x}) = \sum_{i=1}^n B_i(\mathbf{x})a_i + \sum_{j=1}^m P_j(\mathbf{x})b_j = \mathbf{B}^T(\mathbf{x})\mathbf{a} + \mathbf{P}^T(\mathbf{x})\mathbf{b} \quad (14)$$

where a_i is the coefficient for $B_i(\mathbf{x})$ and b_j the coefficient for $P_j(\mathbf{x})$ (usually $m < n$). The definitions of vectors are as follows [18, 19]:

$$\begin{aligned} \mathbf{a}^T &= [a_1, a_2, a_3, \dots, a_n] \\ \mathbf{b}^T &= [b_1, b_2, b_3, \dots, b_m] \\ \mathbf{B}^T(\mathbf{x}) &= [B_1(\mathbf{x}), B_2(\mathbf{x}), B_3(\mathbf{x}), \dots, B_n(\mathbf{x})] \\ \mathbf{P}^T(\mathbf{x}) &= [P_1(\mathbf{x}), P_2(\mathbf{x}), P_3(\mathbf{x}), \dots, P_m(\mathbf{x})] \end{aligned} \quad (15)$$

Basis functions are usually the functions of coordinates $\mathbf{x}^T = [x, y]$ for 2D problems.

The general form of a radial basis function is as follows [18, 19]:

$$B_i(\mathbf{x}) = B_i(r_i) = B_i(x, y) \quad (16)$$

Where r_i is a distance between interpolating point (x, y) and the node (x_i, y_i) . In the Euclidean plane space, this distance is expressed as [18, 19]:

$$r_i = \sqrt{(x - x_i)^2 + (y - y_i)^2} \quad (17)$$

A polynomial basis function has the following monomial terms as [18, 19]:

$$\mathbf{P}^T(\mathbf{x}) = [1, x, y, x^2, xy, y^2, \dots] \quad (18)$$

The interpolation is made to pass through all n scattered nodal points across the influence domain to obtain coefficients a_i and b_j in equation (14).

The interpolation at the k -th point can be obtained by equation (19) [18, 19]:

$$\begin{aligned} u_k = u(x_k, y_k) &= \sum_{i=1}^n a_i B_i(x_k, y_k) + \sum_{j=1}^m b_j P_j(x_k, y_k) \\ &; \quad k = 1, 2, \dots, n \end{aligned} \quad (19)$$

In order to guarantee the uniqueness of approximation, an extra-requirement for the polynomial term is considered [20]. Therefore, the following constraints should be imposed [18, 19]:

$$\sum_{i=1}^n P_j(x_i, y_i) a_i = 0 \quad j = 1, 2, 3, \dots, m \quad (20)$$

It can be expressed in matrix form as follows [18, 19]:

$$\begin{bmatrix} \mathbf{B}_0 & \mathbf{P}_0 \\ \mathbf{P}_0^T & \mathbf{0} \end{bmatrix} \begin{Bmatrix} \mathbf{a} \\ \mathbf{b} \end{Bmatrix} = \mathbf{G} \begin{Bmatrix} \mathbf{a} \\ \mathbf{b} \end{Bmatrix} = \begin{Bmatrix} \mathbf{u}^e \\ \mathbf{0} \end{Bmatrix} \quad (21)$$

Where \mathbf{u}^e is the vector for function values and defined as [18, 19]:

$$\mathbf{u}^e = [u_1, u_2, u_3, \dots, u_n]^T \quad (22)$$

The coefficient matrix \mathbf{B}_0 on unknowns \mathbf{a} is [18, 19]:

$$\mathbf{B}_0 = \begin{bmatrix} B_1(x_1, y_1) & B_2(x_1, y_1) & \dots & B_n(x_1, y_1) \\ B_1(x_2, y_2) & B_2(x_2, y_2) & \dots & B_n(x_2, y_2) \\ \vdots & \vdots & \ddots & \vdots \\ B_1(x_n, y_n) & B_2(x_n, y_n) & \dots & B_n(x_n, y_n) \end{bmatrix} \quad (23)$$

The coefficient matrix \mathbf{P}_0 on unknowns \mathbf{b} is [18, 19]:

$$\mathbf{P}_0 = \begin{bmatrix} P_1(x_1, y_1) & P_2(x_1, y_1) & \dots & P_m(x_1, y_1) \\ P_1(x_2, y_2) & P_2(x_2, y_2) & \dots & P_m(x_2, y_2) \\ \vdots & \vdots & \ddots & \vdots \\ P_1(x_n, y_n) & P_2(x_n, y_n) & \dots & P_m(x_n, y_n) \end{bmatrix} \quad (24)$$

If the inverse of matrix \mathbf{B}_0 exists, a unique solution can be determined [18, 19]:

$$\begin{Bmatrix} \mathbf{a} \\ \mathbf{b} \end{Bmatrix} = \mathbf{G}^{-1} \begin{Bmatrix} \mathbf{u}^e \\ \mathbf{0} \end{Bmatrix} \quad (25)$$

Finally, the interpolation may be expressed as [18, 19]:

$$u(\mathbf{x}) = [\mathbf{B}^T(\mathbf{x}) \quad \mathbf{P}^T(\mathbf{x})] \mathbf{G}^{-1} \begin{Bmatrix} \mathbf{u}^e \\ \mathbf{0} \end{Bmatrix} = \mathbf{\Phi}(\mathbf{x}) \mathbf{u}^e \quad (26)$$

Since the expression $[\mathbf{B}^T(\mathbf{x}) \quad \mathbf{P}^T(\mathbf{x})] \mathbf{G}^{-1}$ is relating the vector of nodal values \mathbf{u}^e to the function field $u(\mathbf{x})$, it is a matrix of shape functions based on the definition of shape function [14, 15].

Therefore the matrix of shape functions is defined by [18, 19]:

$$\mathbf{\Phi}(\mathbf{x}) = [\varphi_1(\mathbf{x}), \varphi_2(\mathbf{x}), \dots, \varphi_i(\mathbf{x}), \dots, \varphi_n(\mathbf{x})] \quad (27)$$

in which [18, 19]:

$$\varphi_k(\mathbf{x}) = \sum_{i=1}^n B_i(\mathbf{x}) \bar{G}_{i,k} + \sum_{j=1}^m P_j(\mathbf{x}) \bar{G}_{n+j,k} \quad (28)$$

Where $\bar{G}_{i,k}$ is the (i, k) element of the matrix \mathbf{G}^{-1} [18, 19].

Now, let us apply the above-mentioned approach utilizing complex Fourier RBFs in a nine node 2D Lagrange element in a natural coordinate system (ξ, η) in order to use in FEM.

5. Complex Fourier elements (CFEs)

In order to obtain shape functions in the two-dimensional CFE, we have to consider the equi-spaced nodes in a 2D natural coordinate system (ξ, η) . The distances between each node to its adjacent nodes in each direction, i.e. ξ and η , are equal to one. For this purpose, first shape functions associated with each node in each direction of the 2D natural coordinate system are obtained; then two shape functions corresponding to each node are multiplied by the following relation [15].

$$\varphi_{3(m-1)+n}(\xi, \eta) = \phi_m(\xi)\phi_n(\eta) \quad (29)$$

Where in equation (29), m is the number of nodes in the natural coordinate system ξ from left to right and n is the number of nodes in the natural coordinate system η from bottom to top. Two-dimensional CFE and one-dimensional CFE in the natural coordinate system are depicted in Figures 3 and 4, respectively [15].

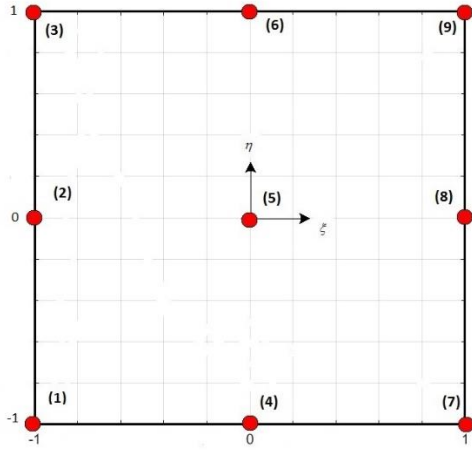


Figure 3. Two-dimensional CFE with 9 nodes in natural coordinate system (ξ, η) [15]

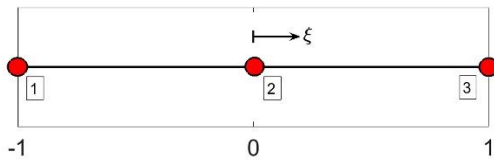


Figure 4. One-dimensional CFE with 3 nodes in the natural coordinate system ξ [14]

For a three-node one-dimensional element, the vectors of complex Fourier RBFs are obtained in relations (a), which are represented by \mathbf{B}_ξ and \mathbf{B}_η in the natural coordinate systems ξ and η , respectively. In relations (b), \mathbf{P}_ξ and \mathbf{P}_η represent vectors of polynomial basis functions for a three-node 1D element in the natural coordinate systems ξ and η , respectively.

$$\mathbf{B}_\xi = \alpha \begin{Bmatrix} e^{i\omega(1+\xi)} \\ e^{i\omega\xi} \\ e^{i\omega(1-\xi)} \end{Bmatrix} \quad \mathbf{B}_\eta = \alpha \begin{Bmatrix} e^{i\omega(1+\eta)} \\ e^{i\omega\eta} \\ e^{i\omega(1-\eta)} \end{Bmatrix} \quad (a)$$

$$\mathbf{P}_\xi = \begin{Bmatrix} 1 \\ \xi \end{Bmatrix} \quad \mathbf{P}_\eta = \begin{Bmatrix} 1 \\ \eta \end{Bmatrix} \quad (b)$$

The following relations are obtained by applying the explained RPIM approach [14, 15]:

$$\begin{aligned} \phi_1(\xi) &= \frac{1}{2}(-\xi + c + h(\xi)); & \phi_1(\eta) &= \frac{1}{2}(-\eta + c + h(\eta)) \\ \phi_2(\xi) &= (1-c) - h(\xi); & \phi_2(\eta) &= (1-c) - h(\eta) \\ \phi_3(\xi) &= \frac{1}{2}(\xi + c + h(\xi)); & \phi_3(\eta) &= \frac{1}{2}(\eta + c + h(\eta)) \end{aligned} \quad (30)$$

In which

$$\begin{aligned} h(\xi) &= \frac{e^{i\omega(1+\xi)} - 2e^{i\omega\xi \text{sgn}(\xi)} + e^{i\omega(1-\xi)}}{(1 - e^{i\omega})(3 - e^{i\omega})} \\ h(\eta) &= \frac{e^{i\omega(1+\eta)} - 2e^{i\omega\eta \text{sgn}(\eta)} + e^{i\omega(1-\eta)}}{(1 - e^{i\omega})(3 - e^{i\omega})} \\ c &= \frac{2}{3 - e^{i\omega}} \end{aligned} \quad (31)$$

Finally, shape functions for the 2D CFE with nine nodes are obtained by the following equations [15]:

$$\begin{aligned} \varphi_1(\xi, \eta) &= \frac{1}{4}(-\xi + c + h(\xi))(-\eta + c + h(\eta)) \\ \varphi_2(\xi, \eta) &= \frac{1}{2}(-\xi + c + h(\xi))(\bar{c} - h(\eta)) \\ \varphi_3(\xi, \eta) &= \frac{1}{4}(-\xi + c + h(\xi))(\eta + c + h(\eta)) \\ \varphi_4(\xi, \eta) &= \frac{1}{2}(\bar{c} - h(\xi))(-\eta + c + h(\eta)) \\ \varphi_5(\xi, \eta) &= (\bar{c} - h(\xi))(\bar{c} - h(\eta)) \\ \varphi_6(\xi, \eta) &= \frac{1}{2}(\bar{c} - h(\xi))(\eta + c + h(\eta)) \\ \varphi_7(\xi, \eta) &= \frac{1}{4}(\xi + c + h(\xi))(-\eta + c + h(\eta)) \\ \varphi_8(\xi, \eta) &= \frac{1}{2}(\xi + c + h(\xi))(\bar{c} - h(\eta)) \\ \varphi_9(\xi, \eta) &= \frac{1}{4}(\xi + c + h(\xi))(\eta + c + h(\eta)) \end{aligned} \quad (32)$$

Where

$$\bar{c} = 1 - c \quad (33)$$

6. Properties of CFEs

Complex Fourier shape functions and elements have the following properties as shown by Khaji and Hamzehei Javaran [14] and Hamzehei-Javaran [15]:

1. Kronecker delta property
2. Partition of unity
3. Infinite piecewise continuity
4. Excellent accuracy in geometry approximation
5. Versatility due to satisfaction of polynomial, trigonometric and exponential function fields simultaneously
6. Perfectly approximation of all kinds of surfaces such as smooth or folded ones
7. No Runge phenomenon
8. Linear independence property
9. Moreover, in the present study, Patch test, including displacement and force patch test, for the 2-D CFEs with nine nodes is assessed and passed.

7. Shape parameters

At first, the motivation for developing approximation techniques using RBFs was to improve accuracy in curve/surface fitting [18]. Even though RBFs have almost half of a century history, the history of the application of them in solving Partial Differential Equations (PDEs) is shorter [19].

For the first time, RBFs were employed to solve the Navier-Stocks equations of fluid flow by Kansa [21, 22]. In his proposed approach, the PDEs directly were discretized over unstructured nodes through Multi-quadric (MQ) basis functions. There were some similarities between his proposed algorithm and finite difference method (FDM), but unlike FDM, node distribution was completely unstructured. He understood that the crucial factor to obtain accurate results was the condition number of the MQ coefficient matrix, which can be adapted through variable shape parameters in the RBFs [19].

The RBFs in the literature usually contain a few shape parameters (from one to four shape parameters) [14]. Generally speaking, in curve/surface fitting through a particular RBF, which has some shape parameters, the use of variable shape parameters can improve the accuracy of the approximation results. The choice of shape parameters has been a hot topic in data fittings [23-26]. In approximation solution of PDEs, the shape parameters mainly represent some constant unknown parameters utilized to enhance the accuracy of RBFs in a specific problem. In other words, for a particular RBF used in a given problem, the best-selected shape parameter would be different for various examples according to the problem's nature such as the type of analysis and applied load. This means that the RBF's user is usually looking for a particular shape parameter that makes the best result for the undertaken problem possible. Hence the best suited shape parameter for a particular problem is regularly chosen by trial-and-error. An alternative approach for finding the unknown parameters of RBFs would be the establishment of an optimization problem [14]. If the exact solution of the problem is known, this solution can be considered as the objective of the optimization problem. Since no exact solutions are available for many practical problems, the approach mentioned above to finding optimum shape parameters for a specific problem is limited to the narrow class of problems.

In the present study, authors employ iso-parametric formulation in the FE code to take advantage of Gaussian quadrature numerical integration. By definition, in the iso-parametric formulation element's geometric shape and displacements within the element are estimated by the same shape functions. [27-29]. We are going

to reduce the number of elements and thus reduce degrees of freedom that are required to solve the problem accurately by using robust elements. To gain this goal, the optimum shape functions have to be found for a particular problem. Shape parameters have the key role in shape functions to achieve this purpose. In this paper, it is proposed based on the experience of authors that in order to find best shape parameters in CFEs, an optimization problem is established in which the geometry of the problem is considered as the objective. The initial concept came to the authors' mind when tried to find an adaptive element that can estimate field variables by only one element and using iso-parametric FE formulation simultaneously, which seems impossible. For this purpose, an optimization code is developed by the authors using Particle Swarm Optimization (PSO) method to reproduce the geometry of the problem by a CFE. Apparently, prior to solving the problem with FEM, it is necessary to solve an optimization problem to adopt the shape parameters. The flowchart of the proposed approach is shown in Figure 5. In the next section in order to demonstrate the robustness of the CFEs in solving viscoelasticity problems, four problems are solved.

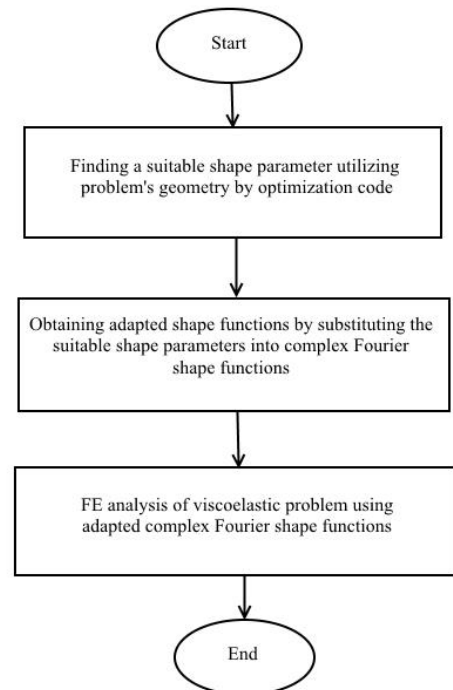


Figure 5. Flowchart of the proposed approach

8. Numerical Examples

In the following section, the accuracy of the proposed method and robustness of the presented elements in viscoelasticity are evaluated through four numerical examples. The convergence rate of FE solution using presented elements toward a common solution is compared with classic FE. The common solution is defined as available analytical or FE results with a fine mesh. All the FE results using commercial software ABAQUS are independent of the mesh. The material property in all illustrative examples is modeled by a Standard Linear Solid (SLS) model, which combines the Maxwell model and a spring in parallel. This model is capable of modeling both relaxation and creep phenomena in viscoelasticity properly. The values of spring constants in the Maxwell element and single parallel spring are 0.4 and 0.1, respectively. The dashpot coefficient in the Maxwell element is 0.4 and Poisson's ratio of the material is assumed to be constant and equal to 0.3.

8.1. Example One. Cantilever Beam with the tip load

A problem of the cantilever beam in Figure 6 is studied here. Consider a beam of length L and height D with values 20 m and 1 m, respectively. The thickness of the beam is 1 m. This example can be considered as a plane stress problem. The beam is subjected to the tip load which is defined by the following expression:

$$P = P_0 [H(t) - H(t - t_1)]; \quad 0 \leq t \leq 40s$$

Where $P_0 = 1N$ and $t_1 = 10s$ and $H(t)$ is well-known Heaviside function. We are looking for the tip displacement w_L .

The loading condition is almost the same as a creep-and-recovery test, but with spatially varying stress and strain. By applying the standard viscoelastic correspondence principle to the elastic solution for tip deflection from solid mechanics, the analytical solution for this example is easily obtained [4, 5, 30]. This approach leads to the following expression for the deflection:

$$w_L = \frac{P_0 L^3}{3I} [D(t) - D(t - t_1)H(t - t_1)] \quad (34)$$

where I is moment of inertia of cross section of the beam and $D(t)$ is the creep compliance. The creep compliance can be easily obtained from Prony series representation of relaxation modulus [5] and is given by:

$$D(t) = D_0 + D_1(1 - e^{-t/\lambda_1}) \quad (35)$$

In which

$$D_0 = \frac{1}{E_0}, \quad E_0 = E_\infty + E_1,$$

$$D_1 = \left(\frac{1}{E_\infty} - \frac{1}{E_0}\right), \quad \lambda_1 = \frac{E_0 \rho_1}{E_\infty}$$

It is noted that even though the solid mechanics solution mentioned above is not exact, it can be accepted as a very good approximation for a beam with an aspect ratio of 20 : 1 [13, 16].

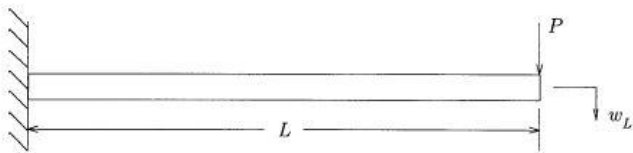


Figure 6. Cantilevered beam's Geometry of Example 1 [13, 16]

The FE meshes used in this example are depicted in Figure 7. Comparison of FE results and the analytical solution is illustrated in Figure 8. At least a mesh consists of 20 classic Lagrange elements is required to FE solution converge to the exact solution. By considering Figure 8, it is obvious that the rate of convergence in quadrilateral CFEs is much higher than classic Lagrange elements. The shape parameter is obtained $\omega = -9i$, based on the mentioned approach in section 7 (Figure 9). In the FE calculations, the time step Δt is assumed to be 0.1 s. It should be noted that the ratio of run time of FE code to obtain accurate results with classic Lagrange elements to CFEs, using an identical personal computer is 10.69. According to the mentioned ratio, it is apparent that CFEs are computationally affordable compared to their classic counterparts, even though required to find the appropriate shape parameter prior to FE analysis.

8.2. Example Two. Encased Cylinder

A long thick-walled viscoelastic pressure vessel encased in a shell of infinite stiffness and under a uniformly distributed internal pressure p is considered as the second example. The geometry of the problem is depicted in Figure 10 which is representative of a solid propellant rocket motor. The problem is regarded as a plane strain case [30]. The internal pressure p is defined by a step load similar to creep test, be given by $p = p_0 H(t)$; $0 \leq t \leq 40s$.

Analytical solution of this problem is obtained by the viscoelastic correspondence principle. The following analytical solution for the radial displacement u_r is easily derived [4, 5]:

$$u_r(r, t) = \frac{p_0 a^2 b(1 + \nu)(1 - 2\nu)}{a^2 + (1 - 2\nu)b^2} \left(\frac{b}{r} - \frac{r}{b}\right) D(t) \quad (36)$$

The quantities of geometry and loading are given by $a = 2m$, $b = 4m$ and $p_0 = 100Pa$ [13, 16].

Closed-form answer and FE results are illustrated in Figure 11 for the radial displacement of the mid-thickness datum. Figure 11 also provides a comparison between the FE results with two different meshes comprising CFEs and classic Lagrange elements. The aforementioned meshes are depicted in Figure 12.

By taking advantage of the symmetry of the problem, merely a quarter of geometry of the problem needs to be modeled. A time increment of 0.1 s is employed in the FE calculations. The shape parameter for this example is obtained $\omega = -0.65 - 1.66i$. Figure 13 compares the problem's geometry and its approximation through complex Fourier interpolation functions utilizing the above-mentioned shape parameter.

As depicted in Figure 11, an excellent agreement exists between the FE results of CFEs, using much fewer elements than classic elements, and closed-form solution. A mesh with at least 49 elements is required to obtain accurate results with classic Lagrange elements (Q9) as shown in Figure 11. Since only two CFEs are required to obtain the excellent results, it is obvious that the run time would be noticeably lower than its classic counterpart to reach similar solutions. The classic Lagrange elements to CFEs run time ratio is 10.51 in executions of the developed code in a similar PC.

8.3. Example three. Elliptic membrane subjected to an outward pressure

A viscoelastic elliptic membrane structure of thickness h , which is subjected to a uniformly distributed outward pressure P , is considered as the third illustrative example (Figure 14). The outward pressure P , is defined by $P = P_0 [H(t) - H(t - t_1)]$; $0 \leq t \leq 30s$ and $t_1 = 10s$.

Symmetry conditions are exploited so that the entire elliptic membrane does not have to be modeled. This problem can be regarded as a plane stress case [30]. The geometric properties and loading of the structure are provided in Table 1. A time increment of 0.1 s is utilized in the FE calculations.

FE results are presented in Figure 15 for the horizontal displacement of the point D. This point is depicted in Figure 14. One of these graphs is obtained by commercial software ABAQUS employing a fine mesh comprises 600 quadrilateral classic elements with midpoints (classic serendipity element Q8). Figure 17 shows the FE mesh used in ABAQUS model. These ABAQUS results are considered as a common solution employed to evaluate the convergence rate of other types of elements. It is worthwhile

to mention that, the ABAQUS software in the analysis of viscoelasticity problems, unlike the developed code by the authors, does not utilize the formulation proposed by Zocher [13].

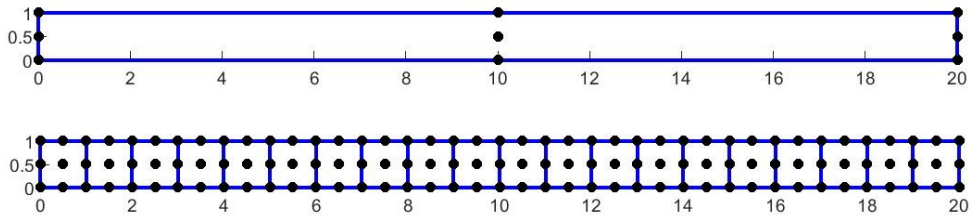


Figure 7. Finite element meshes used in Example 1

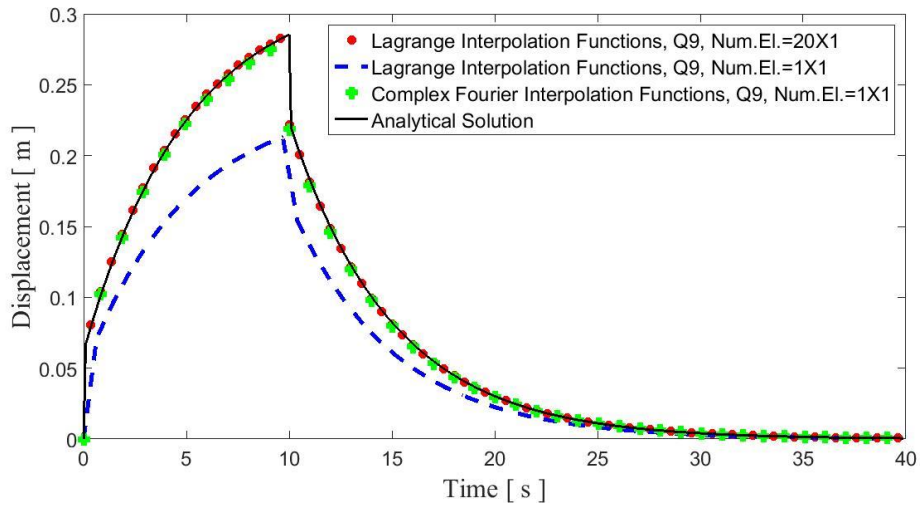


Figure 8. Analytical solution and finite element results with classic Lagrange and Fourier elements in Example 1

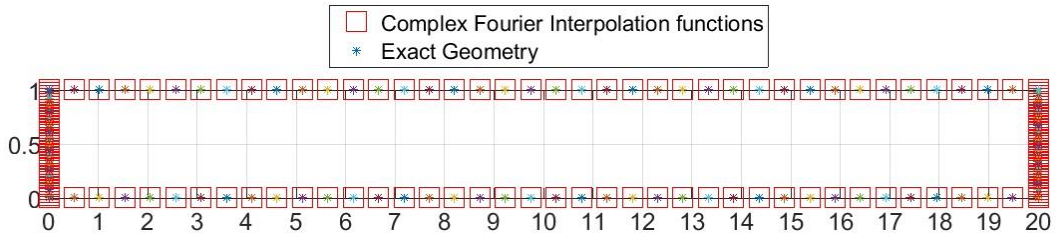


Figure 9. Exact geometry and approximation of geometry of Example 1 using complex Fourier interpolation functions with shape parameter $\omega = -9i$

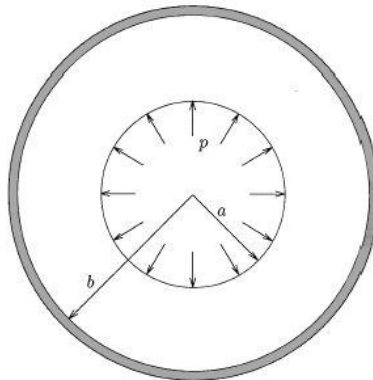


Figure 10. Encased cylinder of Example 2 [13, 16]

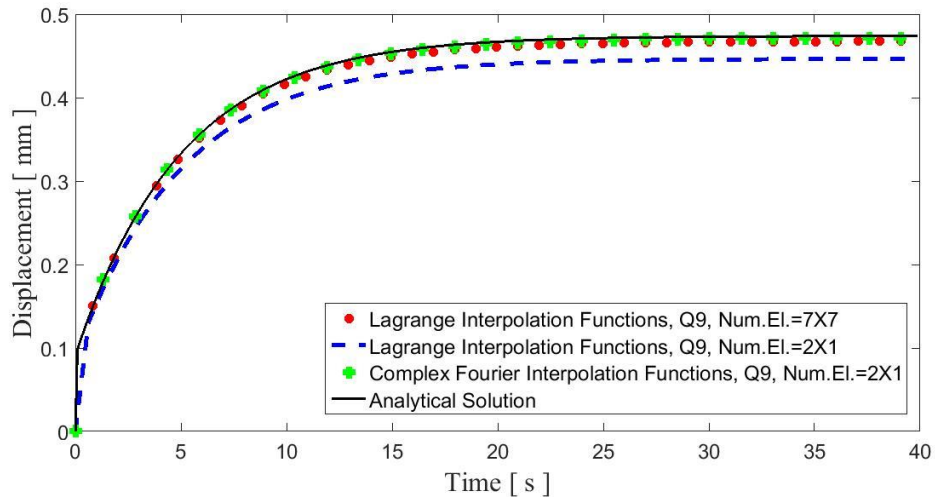


Figure 11. Exact solution and finite element results (radial displacement of the mid-thickness datum) with Lagrange and Fourier elements in Example 2

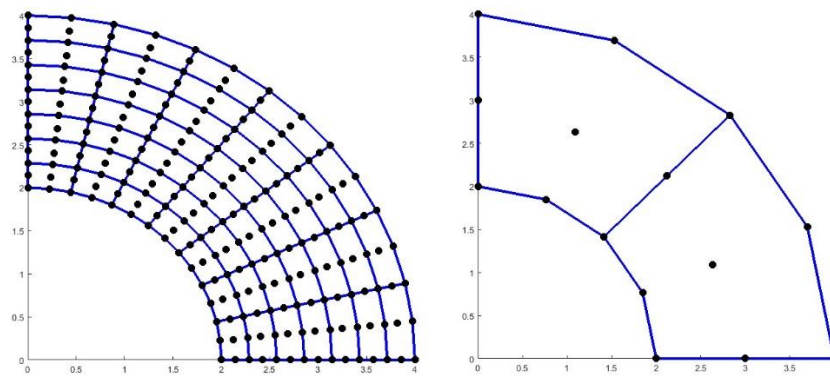


Figure 12. Finite element meshes used in Example 2

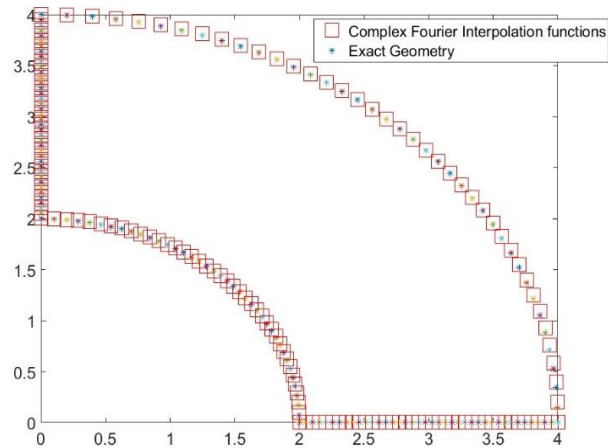


Figure 13. Exact geometry and approximation of geometry with complex Fourier interpolation functions using shape parameter $\omega = -0.65 - 1.66i$ for Example 2

The formulation that is employed by ABAQUS is described in ABAQUS/CAE user's theories manual [31]. In CFEs, the shape parameter is obtained $\omega = 0.98 - 0.5i$, using the optimization code discussed in section 7. The FE meshes utilized in the code for the present example are illustrated in Figure 16.

Table 1. Geometric properties and Loading of the Elliptic membrane [32]

Geometric Properties	Loading
$a = 1.75 \text{ m}$	$P_0 = -10 \text{ MPa}$
$b = 1.0 \text{ m}$	
$c = 2.0 \text{ m}$	
$d = 1.25 \text{ m}$	

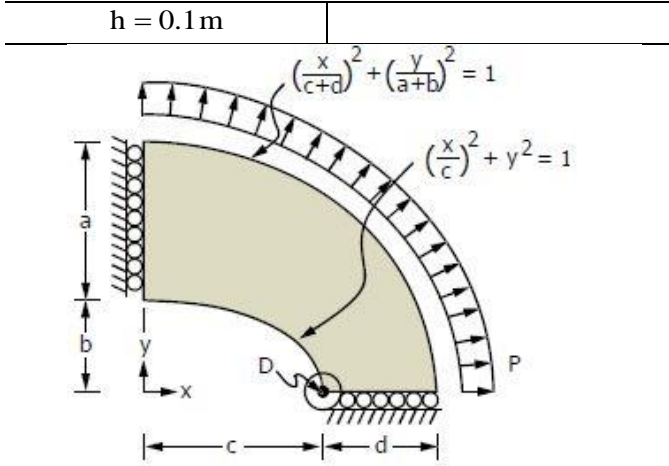


Figure 14. The elliptic membrane of Example 3 [32]

The graph obtained by complex Fourier shape functions with only 16 elements has a perfect agreement with the graph of the common solution, while at least 64 classic Lagrange elements (Q9) is required to reach accurate results, as depicted in Figure 15. The classic Lagrange to CFEs run time ratio is obtained 1.8939, in the execution of the developed code in the similar PC. Therefore CFEs may reduce computational cost efficiently.

8.4. Example Four. Bending of a Curved Beam

A viscoelastic curved beam spans a 90-degree arc as shown in Figure 18 is selected as fourth illustrative example in this paper. The bottom end is supported while the top end is free. The beam is under a clockwise bending moment M applied at the top end. The geometric properties and loading of the curved beam are listed in Table 2. The bending moment at the top end is given by $M = M_0 [H(t) - H(t - t_1)]$; $0 \leq t \leq 10s$ and $t_1 = 4s$ where $H(t)$ is well-known Heaviside function. This problem can be considered as a typical plane stress problem.

Table 2. Geometric properties and Loading of Curved Beam [33]

Geometric Properties	Loading
$r_i = 3.5\text{ m}$	$M_0 = 100\text{ N.m}$
$r_o = 4.5\text{ m}$	
$h = 1.0\text{ m}$	

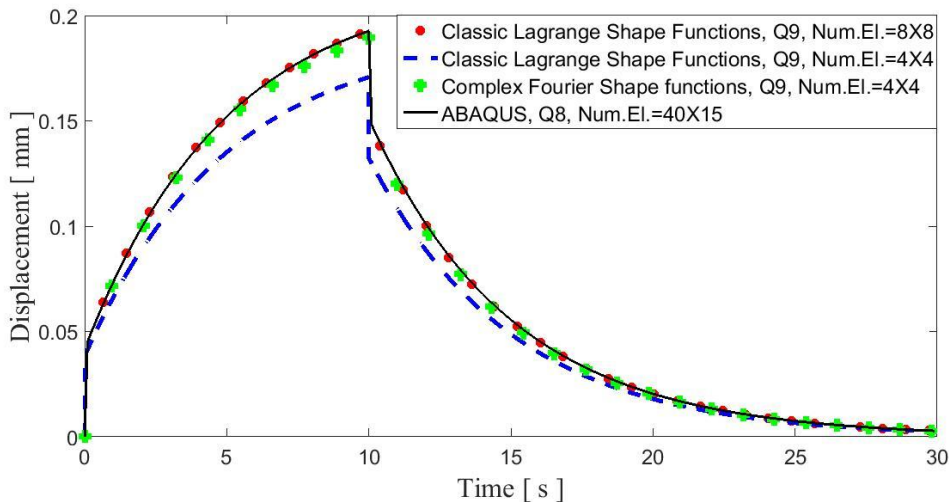


Figure 15. Horizontal displacements of point D obtained by the developed code using complex Fourier and classic Lagrange elements with two different meshes compared with a common solution (ABAQUS) in Example 3

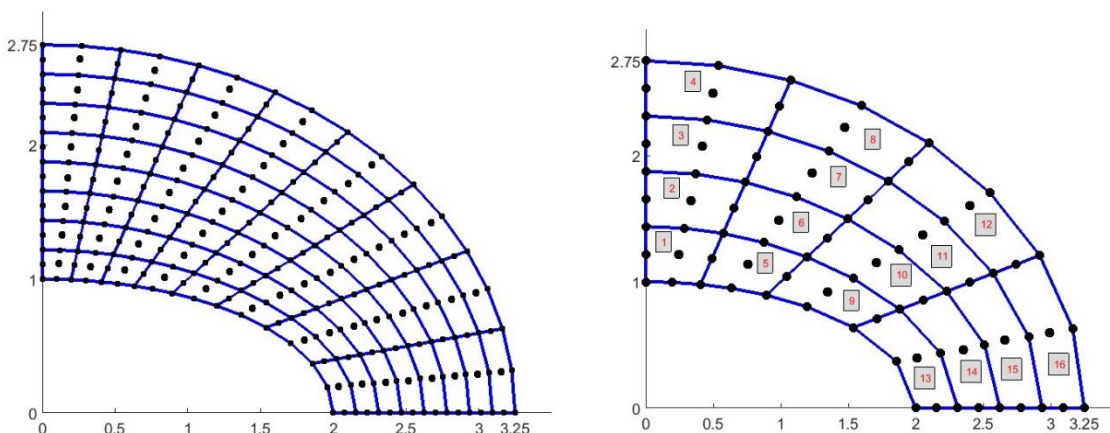


Figure 16. Finite element meshes used in the code for Example 3

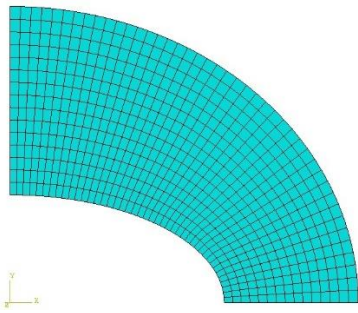


Figure 17. Finite element mesh used in ABAQUS for Example 3

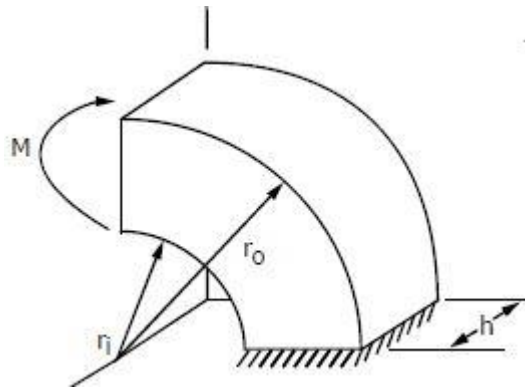


Figure 18. Curved Beam of Example 4 [33]

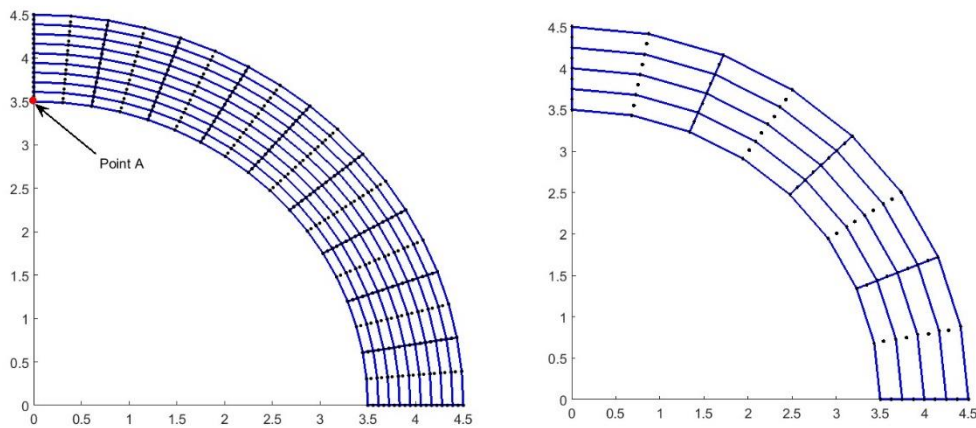


Figure 19. Finite element meshes used in the code for Example 4

FE meshes used in the code for this example are illustrated in Figure 19. In order to obtain a common solution as a basis point to compare convergence of different types of elements, the FE commercial software ABAQUS is employed in this problem, similar to Example 3. The displacements of point A, obtained by ABAQUS utilizing a fine mesh consists of 600 classic quadrilateral serendipity elements Q8 (Figure 20) are shown in Figures 21 and 22. FE analysis is performed using two different meshes consist of 16 CFEs and, 16 and 81 classic Lagrange elements and the results are depicted in Figures 21 and 22. Similar to other examples, the time increment of 0.1 s is used in FE calculations. The shape parameter for this problem is obtained $\omega = -0.65 - 1.66i$ similar to Example 2.

It is apparent from Figures 21 and 22 that, the employment of CFEs can leading to the acceptable solution using the coarse mesh with 16 elements, unlike classic Lagrange elements. The ratio of run time (classic Lagrange to CFEs) to achieve acceptable results is 2.45 in executions of the developed FE program in the same PC. This ratio is reliable evidence for the computational efficiency of the CFEs.

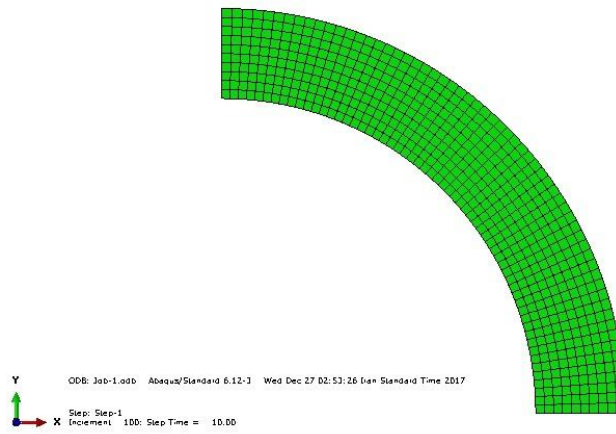


Figure 20. Finite element mesh used in ABAQUS for Example 4

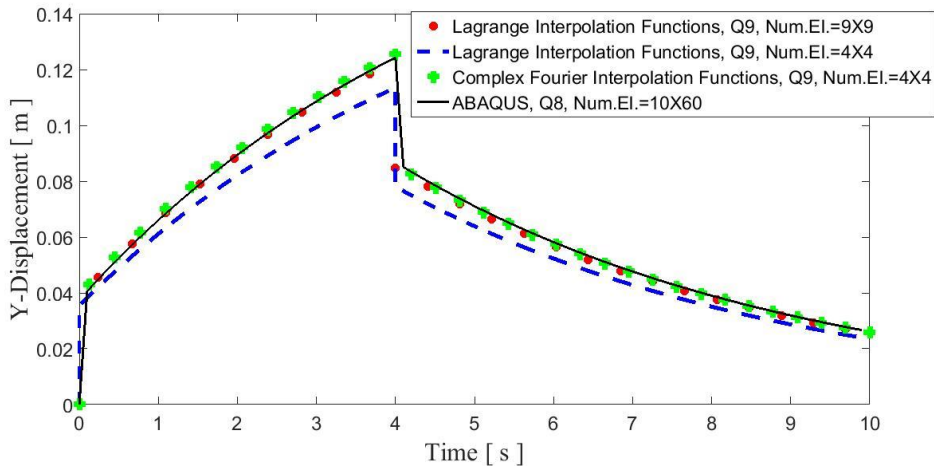


Figure 21. Displacements of point A in Y direction obtained by the developed code using complex Fourier and classic Lagrange elements with two different meshes compared with a common solution (ABAQUS) in Example 4

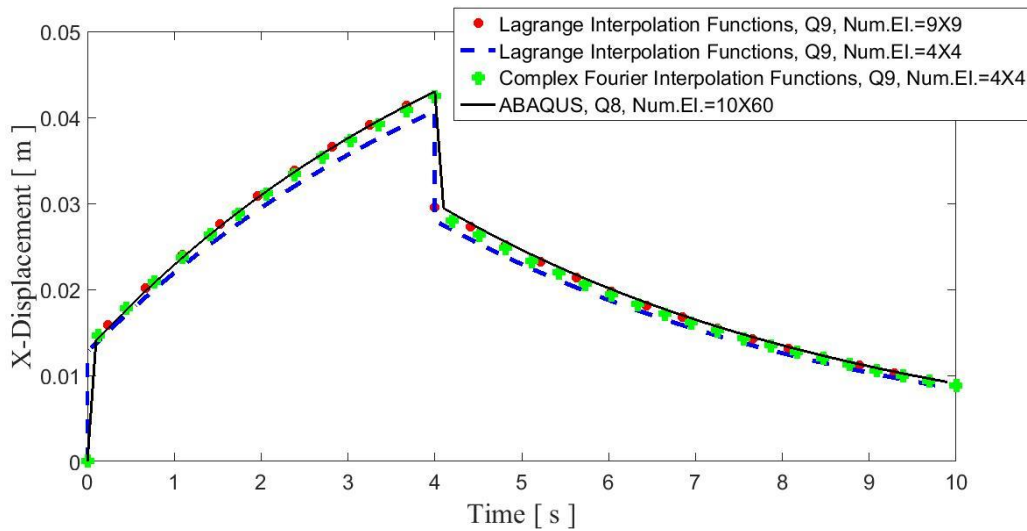


Figure 22. Displacements of point A in X direction obtained by the developed code using complex Fourier and classic Lagrange elements with two different meshes compared with a common solution (ABAQUS) in Example 4

9. Conclusions

In this study, quadrilateral CFEs with nine nodes were employed in the FE analysis of 2D viscoelasticity problems and were compared with conventional FEM. CFEs contain a complex shape parameter which has a crucial role in FE solution.

A finite element code has been developed with the capability of predicting the time-dependent response of viscoelastic materials by the formulation proposed by Zocher using quadrilateral CFEs and classic Lagrange elements. Moreover, an optimization code has been developed by employing the PSO method in order to obtain shape parameter based on the best approximation of the problem's geometry utilizing a CFE.

Four numerical examples were examined and were compared to the results of analytical solution whenever is available, commercial software ABAQUS results and those obtained by classic Lagrange elements to demonstrate the validity and accuracy of the presented approach. In comparison with the classic Lagrange elements, all problems were solved utilizing fewer degrees of freedom with much more accurate results by employing CFEs. This fact can be attributed to the robustness of CFEs which can satisfy various function fields such as exponential, trigonometric and polynomial functions. Moreover, using presented elements made the run time up to ten times shorter than classic elements; therefore CFEs could reduce computational cost efficiently.

References

- [1] Y. Z. Wang, T. J. Tsai, Static and dynamic analysis of a viscoelastic plate by the finite element method, *Applied Acoustics*, Vol. 25, No. 2, pp. 77-94, 1988/01/01/, 1988.
- [2] A. Y. Aköz, F. Kadioğlu, G. Tekin, Quasi-static and dynamic analysis of viscoelastic plates, *Mechanics of Time-Dependent Materials*, Vol. 19, No. 4, pp. 483-503, 2015.
- [3] W. Flügge, 2013, *Viscoelasticity*, Springer Berlin Heidelberg,
- [4] R. Christensen, 2012, *Theory of Viscoelasticity: An Introduction*, Elsevier Science,
- [5] H. F. Brinson, L. C. Brinson, 2015, *Polymer Engineering Science and Viscoelasticity: An Introduction*, Springer US,
- [6] D. Gutierrez-Lemini, 2014, *Engineering viscoelasticity*, Springer,
- [7] N. W. Tschoegl, 2012, *The phenomenological theory of linear viscoelastic behavior: an introduction*, Springer Science & Business Media,
- [8] J. Wang, B. Birgisson, A time domain boundary element method for modeling the quasi-static viscoelastic behavior of asphalt pavements, *Engineering analysis with boundary elements*, Vol. 31, No. 3, pp. 226-240, 2007.
- [9] Q. Xu, M. Rahman, Finite element analyses of layered visco-elastic system under vertical circular loading, *International journal for numerical and analytical methods in geomechanics*, Vol. 32, No. 8, pp. 897-913, 2008.
- [10] G. Ghazlan, S. Caperaa, C. Petit, An incremental formulation for the linear analysis of thin viscoelastic structures using generalized variables, *International journal for numerical methods in engineering*, Vol. 38, No. 19, pp. 3315-3333, 1995.
- [11] J. Sorvari, J. Hämäläinen, Time integration in linear viscoelasticity—a comparative study, *Mechanics of Time-Dependent Materials*, Vol. 14, No. 3, pp. 307-328, 2010.
- [12] I. P. King, *On the finite element analysis of two-dimensional problems with time dependent properties*, Ph.D. Thesis, University of California, Berkeley, USA, 1965.
- [13] M. Zocher, S. Groves, D. H. Allen, A three-dimensional finite element formulation for thermoviscoelastic orthotropic media, *International Journal for Numerical Methods in Engineering*, Vol. 40, No. 12, pp. 2267-2288, 1997.
- [14] N. Khaji, S. H. Javaran, New complex Fourier shape functions for the analysis of two-dimensional potential problems using boundary element method, *Engineering Analysis with Boundary Elements*, Vol. 37, No. 2, pp. 260-272, 2013.
- [15] S. Hamzehei-Javaran, Approximation of the state variables of Navier's differential equation in transient dynamic problems using finite element method based on complex Fourier shape functions, *Asian Journal of Civil Engineering*, pp. 1-20, 2018.
- [16] M. A. Zocher, *A thermoviscoelastic finite element formulation for the analysis of composites*, Ph.D. Thesis, Texas A&M University, USA, 1995.
- [17] M. J. Powell, Radial basis functions in 1990, *Adv. Numer. Anal.*, Vol. 2, pp. 105-210, 1992.
- [18] J. Wang, G. Liu, A point interpolation meshless method based on radial basis functions, *International Journal for Numerical Methods in Engineering*, Vol. 54, No. 11, pp. 1623-1648, 2002.
- [19] J. Wang, G. Liu, On the optimal shape parameters of radial basis functions used for 2-D meshless methods, *Computer methods in applied mechanics and engineering*, Vol. 191, No. 23-24, pp. 2611-2630, 2002.
- [20] M. Golberg, C. Chen, H. Bowman, Some recent results and proposals for the use of radial basis functions in the BEM, *Engineering Analysis with Boundary Elements*, Vol. 23, No. 4, pp. 285-296, 1999.
- [21] E. J. Kansa, Multiquadrics—A scattered data approximation scheme with applications to computational fluid-dynamics—I surface approximations and partial derivative estimates, *Computers & Mathematics with applications*, Vol. 19, No. 8-9, pp. 127-145, 1990.
- [22] E. J. Kansa, Multiquadrics—A scattered data approximation scheme with applications to computational fluid-dynamics—II solutions to parabolic, hyperbolic and elliptic partial differential equations, *Computers & mathematics with applications*, Vol. 19, No. 8-9, pp. 147-161, 1990.
- [23] R. Franke, Scattered data interpolation: tests of some methods, *Mathematics of computation*, Vol. 38, No. 157, pp. 181-200, 1982.
- [24] S. Rippa, An algorithm for selecting a good value for the parameter c in radial basis function interpolation, *Advances in Computational Mathematics*, Vol. 11, No. 2-3, pp. 193-210, 1999.
- [25] R. E. Carlson, T. A. Foley, The parameter R2 in multiquadric interpolation, *Computers & Mathematics with Applications*, Vol. 21, No. 9, pp. 29-42, 1991.
- [26] M. Golberg, C. Chen, S. Karur, Improved multiquadric approximation for partial differential equations, *Engineering Analysis with boundary elements*, Vol. 18, No. 1, pp. 9-17, 1996.
- [27] D. L. Logan, 2011, *A first course in the finite element method*, Cengage Learning,
- [28] J. N. Reddy, 2005, *An introduction to the finite element method*, McGraw-Hill Education, USA, Thirded.
- [29] O. C. Zienkiewicz, 1971, *The Finite Element Method in Engineering Science*, McGraw-Hill Book Co Inc. London, UK
- [30] M. H. Sadd, 2009, *Elasticity: theory, applications, and numerics*, Academic Press,
- [31] D. S. Simulia, ABAQUS CAE Theories Manual, ABAQUS Inc., 2014.
- [32] J. Barlow, G. A. O. Davis, *Selected FE benchmarks in structural and thermal analysis*, Test No. LE1, NAFEMS Report FEBSTA, pp. 1986.
- [33] S. Timoshenko, J. N. Goodier, 1970, *Theory of Elasticity*, McGraw-Hill Book Co. Inc, New York, USA., Thirded.